J Eng Math (2009) 63:241–257
DOI 10.1007/s10665-007-9210-2

The decay of suddenly blocked flow in a curved pipe

Richard J. Clarke · James P. Denier

Received: 21 April 2007 / Accepted: 18 December 2007 / Published online: 10 January 2008

Abstract Pressure-driven viscous flow through a rigid curved pipe of uniform circular cross-section which is suddenly stopped, for example through the instantaneous closure of a valve, is considered here. The profile of the flow at early times after the stoppage is analysed asymptotically, by matching diffusive boundary layers to a core flow that is driven by an axial pressure gradient. This pressure gradient is unknown a priori and, furthermore, exhibits singular behaviour immediately after the stoppage. This analysis therefore provides the flow information at small but finite times that is required for numerical determination of the flow at later times. The limiting case of weak curvature is also considered, where linearization of the governing flow equations is possible. The results illustrate some novel features of the flow which result solely from the pipe's curvature and the consequences for the flow's rate of decay are discussed.

Keywords Blood flow · Curved-pipe flow · Transient flow

1 Introduction

The study of viscous flow through a curved pipe has relevance to a great number of different areas and, as such, has been a subject of fluid-dynamical interest for many years. Physiological interests have been an especially strong source of stimulation [1], as a proper understanding of blood flow within veins and arteries can provide useful insights into clinical conditions such as atherosclerosis, which are believed to be a function of the shear stresses exerted by the fluid on the vessel walls [2]. One of the earliest theoretical treatments of pressure-driven flow of a viscous fluid through a curved pipe was given in [3], where a series solution was constructed for the time-independent flow through a weakly curved pipe that is driven by a moderate pressure gradient. (A weakly curved pipe is one where the radius of curvature R, i.e., the radius of the circle that contains the arc defining the pipe's centreline, is much smaller than the radius of the pipe's cross-section a; see Fig. 1. It will prove useful to define a dimensionless curvature parameter $\delta \equiv a/R$.) An important feature of curved-pipe flow is the centrifugally driven secondary flow within the cross-section of the pipe, which understandably has consequences for the transport properties of the flow [4]. Subsequent numerical investigations into the steady weak curvature limit have revealed the existence of symmetry-breaking bifurcations in the flow profile when the axial pressure gradient is sufficiently high, which

R. J. Clarke (✉) · J. P. Denier
School of Mathematical Sciences, University of Adelaide, Adelaide, SA 5005, Australia
e-mail: richard.clarke@adelaide.edu.au

results in a multiplicity of steady states [5]. Allowing the pipe to have finite curvature, in order to model significantly curved pipes such as the aorta, introduces Coriolis effects in addition to the centrifugal forces present in the weak curvature limit, and this has been shown to have consequences for the structure of the flow and the shear stresses exerted by the fluid on the pipe wall [6]. Further geometric generalisations include flow through a helix, where the pipe has torsion as well as curvature [7], as well as flow through pipes with a time-dependent curvature [8].

Recognising that true arterial flow is driven by the heart in a time-dependent manner, flow in a weakly curved pipe driven by an oscillatory pressure gradient was considered in [9]. The flow under these circumstances is more complex, with steady-streaming effects driving flows in the pipe cross-section which act in an opposite direction to the centrifugally driven secondary flows. The more general case of pulsatile flow (oscillatory flow about a non-zero mean) in weakly curved pipes has been treated in [10] and through finite-curvature pipes in [11]. Pulsatile flow itself is an idealisation of the typically intermittant flows in the aorta, where a pulse-like volumetric flow rate during the *systolic* phase is followed by a *diastolic* period of zero volumetric flow rate. For a straight pipe, the extreme case where a constant flow rate is instantly reduced to zero has been treated in [12], where analytic progress was made in describing the ensuing post-stoppage flow. Despite the idealised nature of this flow, it has been shown to exhibit some of the important features observable in recent full numerical simulations [13], which used a pulse-like flow-rate waveform. For example, observations of points of inflection in the streamwise velocity profiles due to reversal of the flow near the wall, which are often the markers for flow instability, as illustrated by classical stability analysis [14]. Such analysis, however, requires a sufficiently high Reynolds number for separation of timescales between the base flow and the perturbations, but not so high as to eradicate viscous effects. With the aim of relaxing these conflicting requirements on the Reynolds number, and acknowledging the importance of transient effects [15], the stability of suddenly stopped straight-pipe flow was recently re-analysed using an explicit-transient analysis of the time-dependent decaying flow [16], which revealed significant differences in the critical Reynolds numbers for transition to turbulence from that predicted using classical stability theory.

The straight-pipe limit, however, is not able to reproduce all of the interesting and potentially important flow phenomena observed in the numerical experiments [13]. By extending the suddenly stopped analysis to curved pipes, we hope to give quantitative insight into some of the laminar features that are attributable to curvature effects, as well as to lay the groundwork for subsequent stability analysis.

Suddenly stopped flow in a pipe is also of great industrial importance, with a traditional area of interest being the study of the generated pressure waves and their well-documented ability to cause pipe damage (e.g. the *water-hammer* effect). Some modern innovations, such as novel methods for detecting leaks in pipelines [17], are now demanding a better understanding of viscous flow effects within suddenly stopped pipe flow. These considerations may also be relevant when determining how sudden stoppages can lead to fluid contamination via leakage through joints or cracks, or perhaps the stripping and mixing of a biofilm through strongly induced shear stresses on the pipe wall [18].

In Sect. 2 we introduce the governing equations, and then go on to complete the specification of the initial conditions for the post-stoppage flow by asymptotically analysing their small-time behaviour in Sect. 3. This is followed in Sect. 4 by consideration of the weak-curvature limit. Evolution of the flow at later times must be determined numerically and the computational scheme for achieving this is laid out in Sect. 5. Results are presented in Sect. 6 with conclusions and implications then discussed in Sect. 7.

2 Formulation

We consider a pipe with constant cross-sectional radius a and constant radius of curvature R, filled with an incompressible fluid of density ρ and viscosity ν. We use a curvilinear coordinate system (r^*, θ, ϕ), defined by

$$x^* = (r^* \cos\theta + R)\sin\phi, \quad y^* = (r^* \cos\theta + R)\cos\phi, \quad z^* = r^* \sin\theta$$

(note that an asterisk denotes a dimensional variable) with respect to Cartesian coordinates (x^*, y^*, z^*). A sketch of the geometry is laid out in Fig. 1. The flow $\boldsymbol{u}^* = (u^*, v^*, w^*)$ therefore consists of radial, azimuthal and axial components, respectively.

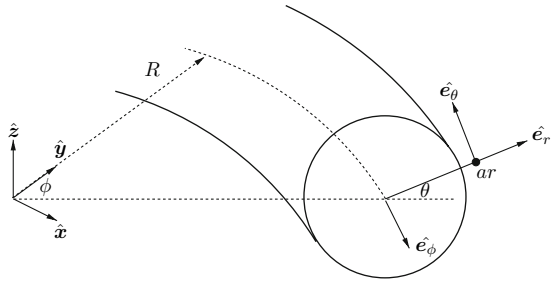

Fig. 1 Flow in a curved pipe of uniform cross-sectional radius a is described using a (dimensionless) curvilinear coodinate system (ar, θ, ϕ). The pipe is assumed to have a constant radius of curvature R

The blockage occurs instantly at time $t^* = 0$ and we consider the flow at a suitably large distance from the source of the blockage such that we may assume the flow is fully developed (i.e., ϕ-independent). For a straight pipe, the flow typically becomes fully developed at $O(a\mathrm{Re})$ distances from the pipe entrance (where Re is a Reynolds number $W_e a/\nu$ based on a typical flow velocity W_e at the pipe entrance). For a curved pipe, however, the lengthscale over which steady flow develops (the entry length) depends upon the strength of centrifugal effects, as measured by the quantity $\delta^{1/2}G_0$, where G_0 is a characteristic axial pressure gradient through the pipe. When centrifugal effects are large, the entry length reduces from an $O(a\mathrm{Re})$ distance (i.e., as in a straight pipe) to an $O(\mathrm{Re}^{1/2}\delta^{-1/4})$ distance, due to the improved transport of vorticity and momentum across the pipe via secondary flows. An overview of entry flow in curved pipes is given in [1].

As for the straight-pipe flow considered in [12], we expect viscous diffusion to dominate the evolution of the post-stoppage flows. We therefore scale radial distance on a, flow velocities on ν/a, pressure on $\nu^2\rho/a^2$, time on a^2/ν. The non-dimensional momentum equations for the flow then take the following form [19, p. 162]:

$$\partial_t u + u\partial_r u + \frac{v\partial_\theta u}{r} - \frac{v^2}{r} - \frac{\delta\cos\theta w^2}{h} = -\partial_r p - \frac{1}{rh}\partial_\theta\left[h\left(\partial_r v + \frac{v}{r} - \frac{\partial_\theta u}{r}\right)\right], \tag{1a}$$

$$\partial_t v + u\partial_r v + \frac{v\partial_\theta v}{r} + \frac{uv}{r} + \frac{\delta\sin\theta w^2}{h} = -\frac{\partial_\theta p}{r} + \frac{1}{h}\partial_r\left[h\left(\partial_r v + \frac{v}{r} - \frac{\partial_\theta u}{r}\right)\right], \tag{1b}$$

$$\partial_t w + u\partial_r w + \frac{v\partial_\theta w}{r} + \frac{\delta\cos\theta uw}{h} - \frac{\delta\sin\theta vw}{h} = \frac{G(t)}{h} + \mathcal{L}^2 w, \tag{1c}$$

where $h = 1+\delta r\cos\theta$, $-G(t)$ is the time-dependent axial pressure gradient scaled on $\rho\nu^2/a^3$ (necessarily spatially independent through the fully developed assumption) and

$$\mathcal{L}^2 = \partial_{rr}^2 + \left(\frac{1}{rh} + \frac{2\delta\cos\theta}{h}\right)\partial_r + \frac{1}{r^2}\partial_{\theta\theta}^2 - \frac{\delta\sin\theta\partial_\theta}{hr} - \frac{\delta^2}{h^2}. \tag{1d}$$

These are supplemented by the continuity equation

$$\partial_r u + \frac{u(1+2\delta r\cos\theta)}{rh} + \frac{\partial_\theta v}{r} - \frac{v\delta\sin\theta}{h} = 0. \tag{1e}$$

We are required to solve (1) subject to the boundary conditions

$$u(1,\theta,t>0) = 0, \quad v(1,\theta,t>0) = 0, \quad w(1,\theta,t>0) = 0. \tag{2}$$

The fully developed nature of the flow, however, allows us to simplify the flow equations by introducing a stream function $\psi(r,\theta,t)$ which satisfies

$$u = h^{-1}r^{-1}\partial_\theta\Psi, \quad v = -h^{-1}\partial_r\Psi, \quad \Psi = h\psi. \tag{3}$$

We also eliminate cross-sectional pressure gradients by recasting (1a,b) into the form

$$\partial_t\omega + \frac{1}{r}\left(\frac{\partial_r\omega\partial_\theta\Psi}{h} - \frac{\delta\cos\theta\omega\partial_\theta\Psi}{h^2} - \frac{\partial_r\Psi\partial_\theta\omega}{h} - \frac{\delta r\sin\theta\omega\partial_r\Psi}{h^2}\right)$$
$$- \frac{2\delta w\sin\theta\partial_r w}{h} - \frac{2\delta w\cos\theta\partial_\theta w}{hr} = \mathcal{L}^2\omega, \quad \omega = \mathcal{L}^2\psi, \tag{4}$$

where $\omega = -\xi$ is the negative of the axial component of vorticity ξ. Under the fully developed flow assumption, use of the stream function ensures conservation of mass automatically. The boundary conditions (2a,b) are converted into the following stream function form:

$$\psi(1, \theta, t > 0) = \partial_r \psi(1, \theta, t > 0) = 0. \tag{5}$$

In addition, the blockage imposes a zero flux condition through the pipe

$$Q(t > 0) = \int_0^{2\pi} \int_0^1 r w(r, \theta, t) \mathrm{d}r \mathrm{d}\theta = 0, \tag{6}$$

and the pressure gradient $G(t)$ is chosen to enforce this no-flux condition and hence must be determined at the same time as the flow.

Just as for a straight pipe [12], the new boundary condition at the source of the blockage is enforced through the propagation of a pressure wave through the pipe. On the diffusive timescale this results in unphysical jumps in certain flow quantities, such as the flux and the axial pressure gradient. These jumps, however, are smoothed out on a much shorter $O(a/c)$ timeframe (with c the velocity of sound in the fluid) close to the instant that the pipe becomes blocked. We determine whether there is any possible jump in the vorticity on the diffusive timescale by analysing the Navier–Stokes vorticity equation over this short timescale

$$\frac{\partial \boldsymbol{\omega}}{\partial t} - M \boldsymbol{\nabla} \times (\boldsymbol{u} \times \boldsymbol{\omega}) = -\frac{M}{\mathrm{Re}} \boldsymbol{\nabla} \times \boldsymbol{\nabla} \times \boldsymbol{\omega}, \tag{7}$$

where $M = U_c/c$ and $\mathrm{Re} = U_c a/\nu$ (where U_c is a typical centreline velocity for the flow). We see that when pre-stoppage flow velocities are sufficiently slower than the speed of sound ($M \ll 1$)

$$\frac{\partial \boldsymbol{\omega}}{\partial t} = \mathbf{0}, \tag{8}$$

the vorticity distribution is unchanged during the passage of the pressure wave. Hence there is no jump in the vorticity on the diffusive timescale and so it takes the pre-stoppage value, i.e., the flow initially adjusts in an irrotational manner to the presence of the blockage. The flow profile immediately after the blockage therefore satisfies

$$\boldsymbol{\nabla} \times \boldsymbol{u}|_{t=0} = \boldsymbol{\omega}^-,$$

where $\boldsymbol{\omega}^-$ is the pre-blockage vorticity distribution, i.e., the initial vorticity of the post-stoppage flow is equal to the vorticity of the pre-stoppage flow, but now the flow is subject to a condition of zero net flow through the pipe. In this paper we consider the pre-stoppage flow to be fully developed incompressible steady flow $\boldsymbol{u}_D$ in a finitely curved pipe, driven by a time-independent axial pressure gradient. The structure of these pre-stoppage flows has recently been analysed in some detail [6].

Let us write the initial velocity as a correction $\bar{\boldsymbol{u}}$ to the pre-stoppage fully developed flow $\boldsymbol{u}_D(r, \theta)$

$$\boldsymbol{u}|_{t=0} = \boldsymbol{u}_D|_{t=0} + \bar{\boldsymbol{u}},$$

so that

$$\boldsymbol{\omega}^+ = \boldsymbol{\nabla} \times \boldsymbol{u}|_{t=0} = \boldsymbol{\omega}^- + \boldsymbol{\nabla} \times \bar{\boldsymbol{u}},$$

where $\boldsymbol{\omega}^+$ is the initial post-blockage vorticity distribution. Since $\boldsymbol{\omega}^- = \boldsymbol{\omega}^+$ we must have $\boldsymbol{\nabla} \times \bar{\boldsymbol{u}} = \mathbf{0}$. As the flow domain is simply connected, there exists a single-valued flow potential $\bar{\Phi}$ such that $\bar{\boldsymbol{u}} = \boldsymbol{\nabla} \bar{\Phi}$. Conservation of mass implies $\boldsymbol{\nabla} \cdot \bar{\boldsymbol{u}} = 0$ (since the pre-stoppage flow $\boldsymbol{u}_D$ is divergence-free), hence

$$\nabla^2 \bar{\Phi} = 0. \tag{9}$$

Now from the fully developed assumption, $\bar{\Phi}$ must have the form

$$\bar{\Phi} = -\alpha \phi + \bar{f}(r, \theta),$$

where α is a constant that will be determined through the no-flux condition and $\bar{f}$ is an as yet unknown function. However, on substitution in (9) we have

$$\nabla^2 \bar{f} = 0. \tag{10}$$

Now consider a region of the flow bounded by the pipe wall and two arbitrary cross-sectional planes, at $\phi = \phi_2$ and $\phi = \phi_1$ ($\phi_2 > \phi_1$). At the pipe wall and the two cross-sectional planes the derivatives of $\bar{f}$ in directions normal to the surface are zero, through the no-penetration condition at $r = 1$ and through the form for $\bar{\Phi}$, as given by (10), at $\phi = \phi_1$ and ϕ_2. Hence, within the volume

$$\bar{f}(r, \theta) = 0$$

(up to an irrelevant constant). Since the choice of ϕ_1 and ϕ_2 was arbitrary, $\bar{f}(r, \theta)$ is zero everyehere. We are therefore left with the following initial conditions on the flow velocity

$$u(r, \theta, 0) = u_D(r, \theta), \quad v(r, \theta, 0) = v_D(r, \theta), \quad w(r, \theta, 0) = w_D(r, \theta) - \alpha h^{-1}, \tag{11}$$

recalling that $\boldsymbol{u}_D$ is the fully developed steady pre-stoppage flow satisfying (1) driven by a constant axial pressure gradient $G(t) = D$, e.g. $P(r, \theta, \phi) = D\phi + p_D(r, \theta)$.

In stream function form, the initial condition for the cross-sectional flow becomes

$$\psi(r, \theta, 0) = \psi_D(r, \theta), \tag{12}$$

where ψ_D is the stream function for the cross-sectional components of $\boldsymbol{u}_D(r, \theta)$. Note that to satisfy no-flux at $t = 0$,

$$\alpha = \frac{\delta^2 Q_D}{2\pi(1 - \sqrt{1 - \delta^2})},$$

where Q_D is the pre-stoppage flow's flux which, in general, must be computed numerically. For later analysis it proves useful to note that $\alpha \to Q_D/\pi = D/8$ as $\delta \to 0$. In order to fully specify the problem we require initial conditions for $G(t)$, which must be determined through analysis of the small-time behaviour of the flow.

3 The small-time limit

In what follows we rescale time $t = \epsilon T$ ($\epsilon \ll 1$, $T = O(1)$) and, in anticipation of the similarity form for a vortex sheet that forms on the pipe walls in response to the initial axial slippage (11), we expand both the velocity and pressure in powers of $\epsilon^{1/2}$:

$$\boldsymbol{u} = \boldsymbol{u}^{(0)} + \epsilon^{1/2}\boldsymbol{u}^{(1)} + \epsilon\boldsymbol{u}^{(2)} + \cdots,$$
$$p = \epsilon^{-1}G^{(0)}(T)\phi + \epsilon^{-1/2}G^{(1)}(T)\phi + (G^{(2)}(T)\phi + p^{(2)}(r, \theta)) + \cdots.$$

We expect this vortex sheet to diffuse into the core over time, and so choose to decompose the flow into a core contribution $\hat{\boldsymbol{u}}$, together with a diffusive boundary-layer flow $\tilde{\boldsymbol{u}}$. Detailed calculations of the flows in these two distinct asymptotic regions are given in Appendix A, which match together to form the following uniform-valid expression for the post-stoppage flow at small times (up to $O(\epsilon^{3/2})$ corrections)

$$u = u_D + t\left[-\partial_r \hat{P}^{(2)} - \frac{2\alpha\delta\cos\theta w_D}{h^2} + \frac{\alpha^2\delta\cos\theta}{h^3}\right], \tag{13a}$$

$$v = v_D + t\left[-\frac{1}{r}\partial_\theta \hat{P}^{(2)} + \frac{2\alpha\delta\sin\theta w_D}{h^2} - \frac{\alpha^2\delta\sin\theta}{h^3} + K(r, \theta) + \frac{\alpha^2\delta\sin\theta}{h_1^3}\right], \tag{13b}$$

$$\begin{aligned} w = {} & \left[w_D - \frac{\alpha}{h} + \frac{\alpha}{h_1}\mathrm{erfc}\eta\right] + t^{1/2}\left[\frac{2\bar{G}^{(1)}}{h} + \frac{2\bar{G}^{(1)}}{h_1}\left(\sqrt{\pi}\eta\,\mathrm{erfc}\eta - e^{-\eta^2}\right) + \alpha\frac{(1 + 2\delta\cos\theta)}{h_1^2}\eta\,\mathrm{erfc}\eta\right] \\ & + t\left[\frac{G^{(2)}}{h} - \frac{D}{h} - \left(\frac{G^{(2)}}{h_1} - \frac{D}{h_1}\right)\left((1 + 2\eta^2)\mathrm{erfc}\eta - \frac{2\eta e^{-\eta^2}}{\sqrt{\pi}}\right)\right. \\ & \left. + f_2(\theta)\eta e^{-\eta^2} + \left(A_1(r, \theta) - \frac{2\alpha\delta^2\cos^2\theta}{h_1^3}\right)\left(\frac{2\eta e^{-\eta^2}}{\sqrt{\pi}} - 2\eta^2\mathrm{erfc}\eta\right)\right], \end{aligned} \tag{13c}$$

where functions K, f_2 and A_1 are given by (35), (32) and (34a), respectively; $G^{(1)} = T^{-1/2}\bar{G}^{(1)}$, $h_1 = 1 + \delta\cos\theta$ and $\hat{P}^{(2)}$ ensures conservation of mass (23c,d).

The unknown axial pressure gradients $\bar{G}^{(1)}$ and $G^{(2)}$ are now determined through enforcement of the no-flux condition. The leading-order boundary-layer flow $\tilde{\boldsymbol{u}}^{(0)}$ produces the following flux through the pipe's cross-section (correct up to exponentially small terms in ϵ)

$$Q^{(0)} = \int_0^{2\pi}\int_0^1 w^{(0)}\, r\mathrm{d}r\mathrm{d}\theta = \epsilon^{1/2}Q^{(00)} + \epsilon Q^{(01)}, \tag{14a}$$

where

$$Q^{(00)} = \frac{4\alpha\sqrt{\pi}T^{1/2}}{\sqrt{1-\delta^2}}, \quad Q^{(01)} = -\frac{2\alpha\pi T}{\sqrt{1-\delta^2}}. \tag{14b}$$

Requiring that the $O(\epsilon^{1/2})$ core flow $\hat{\boldsymbol{u}}^{(1)}$ cancels the $O(\epsilon^{1/2})$ flux $Q^{(00)}$ from $\tilde{\boldsymbol{u}}^{(0)}$

$$\int_0^{2\pi}\int_0^1 \hat{w}^{(1)} r\mathrm{d}r\mathrm{d}\theta = \int_0^{2\pi}\int_0^1 \frac{2\bar{G}^{(1)}T^{1/2}}{h} r\mathrm{d}r\mathrm{d}\theta = -Q^{(00)},$$

gives us the leading-order pressure gradient

$$\bar{G}^{(1)} = \frac{\alpha\delta^2}{\sqrt{\pi}(\sqrt{1-\delta^2}-1)\sqrt{1-\delta^2}} \to -D/(4\sqrt{\pi}) \quad \text{as } \delta \to 0,$$

in agreement with the straight-pipe results [16]. The flux generated by the $O(\epsilon^{1/2})$ boundary-layer flow $\tilde{\boldsymbol{u}}^{(1)}$ (correct up to $O(\epsilon^{3/2})$) is given by

$$Q^{(1)} = \int_0^{2\pi}\int_0^1 \tilde{w}^{(1)}\, r\mathrm{d}r\mathrm{d}\theta = \epsilon T\left(\frac{-2\pi^{3/2}\bar{G}^{(1)}}{\sqrt{1-\delta^2}} + \alpha\pi\frac{(1-2\delta^2)}{(1-\delta^2)^{3/2}}\right), \tag{15}$$

such that $Q^{(1)} \to 5D\pi/8$ as $\delta \to 0$. The $O(\epsilon)$ core flow $\hat{\boldsymbol{u}}^{(2)}$ must be chosen such that the resulting flow cancels out the flux $Q^{(01)}$ in (14) induced by the leading-order boundary-layer flow $\tilde{\boldsymbol{u}}^{(0)}$, plus the above computed flux $Q^{(1)}$ induced by the second-order boundary-layer flow

$$\int_0^{2\pi}\int_0^1 \hat{w}^{(2)}\, r\mathrm{d}r\mathrm{d}\theta = T\int_0^{2\pi}\int_0^1 \frac{G^{(2)}}{h} r\mathrm{d}r\mathrm{d}\theta + Q^{(21)} = -Q^{(01)} - Q^{(1)},$$

where

$$Q^{(21)} = -T\int_0^{2\pi}\int_0^1 \frac{D}{h} r\mathrm{d}r\mathrm{d}\theta = \frac{-2\pi T D(1-\sqrt{1-\delta^2})}{\delta^2} \to -\pi T D \quad \text{as } \delta \to 0.$$

The appropriate pressure gradient is therefore

$$G^{(2)} = \frac{\delta^2(Q^{(01)} + Q^{(1)} + Q^{(21)})}{2\pi(\sqrt{1-\delta^2}-1)},$$

which approaches $5D/8$ as $\delta \to 0$, once more in agreement with the straight-pipe results [16]. The agreement of the small-time asymptotics against full numerical solutions is assessed in Sect. 6.

4 The small-curvature limit ($\delta \ll 1$)

In general, for finite curvature, we must compute the initial condition $w_D - \alpha h^{-1}$ numerically, which limits the extent to which we can express the small-time approximation of Sect. 3 in closed form. When the pipe is only weakly curved, however, we can exploit previously derived asymptotic approximations to $\boldsymbol{u}_D$, which can be used in conjunction with small-curvature asymptotic analysis to describe the weakly curved pipe flow at all times after the stoppage. Therefore, in the small-curvature limit, we seek an expansion of the form:

$$\boldsymbol{u} = \boldsymbol{u}_0 + \delta\boldsymbol{u}_1 + \cdots, \quad G = (G_0\phi + p_0) + \delta(G_1\phi + p_1) + \cdots$$

The $O(1)$ flow is then governed by

$$\partial_t u_0 + u_0\partial_r u_0 + \frac{v_0\partial_\theta u_0}{r} - \frac{v_0^2}{r} = -\partial_r p_0 - \frac{1}{r}\partial_\theta\left(\partial_r v_0 + \frac{v_0}{r} - \frac{\partial_\theta u_0}{r}\right), \tag{16a}$$

$$\partial_t v_0 + u_0\partial_r v_0 + \frac{v_0\partial_\theta v_0}{r} + \frac{u_0 v_0}{r} = -\frac{\partial_\theta p_0}{r} + \partial_r\left(\partial_r v_0 + \frac{v_0}{r} - \frac{\partial_\theta u_0}{r}\right), \tag{16b}$$

$$\partial_t w_0 + u_0\partial_r w_0 + \frac{v_0\partial_\theta w_0}{r} = G_0(t) + \frac{1}{r}\left(\frac{\partial_\theta^2 w_0}{r} + \partial_r\left(r\partial_r w_0\right)\right), \tag{16c}$$

$$\partial_r u_0 + \frac{u_0}{r} + \frac{\partial_\theta v_0}{r} = 0, \tag{16d}$$

subject to [6]

$$\boldsymbol{u}_0(1,\theta,t>0) = \mathbf{0}, \quad u_0(r,\theta,0) = v_0(r,\theta,0) = 0, \quad w_0(r,\theta,0) = \frac{1}{4}D(1-r^2), \tag{16e}$$

which is the straight-pipe problem considered in [12]. The decay of the $O(\delta)$ flow, in axial velocity–stream-function form, is governed by

$$\partial_t w_1 - \nabla_p^2 w_1 = G_1(t) - r\cos\theta G_0(t) - u_1\partial_r w_0 - \frac{\sin\theta}{r}\partial_\theta w_0 + \cos\theta\partial_r w_0, \tag{17a}$$

$$\partial_t \nabla_p^2\psi_1 - \nabla_p^4\psi_1 = \sin\theta\partial_r\left(w_0^2\right), \tag{17b}$$

(where $\nabla_p^2 \equiv \frac{1}{r}\partial_r(r\partial_r) + \frac{1}{r^2}\partial_\theta^2$ is the two-dimensional Laplacian in polar coordinates). We are required to solve (17) subject to the no-flux constraint (6) and

$$\psi_1(1,\theta,t>0) = \partial_r\psi_1(1,\theta,t>0) = w_1(1,\theta,t>0) = 0, \tag{18a}$$

$$\psi_1(r,\theta,0) = 2D^2c_1^{-1}r(1-r^2)^2(4-r^2)\sin\theta, \tag{18b}$$

$$w_1(r,\theta,0) = \left(-\frac{3}{16}r(1-r^2) + \frac{1}{c_2}(r-r^3)(19-21r^2+9r^4-r^6)\right)D\cos\theta, \tag{18c}$$

[6] where $c_1 = 2^{10}\times 9$, $c_2 = 2^{15}\times 45$. Although, in general, (16)–(18) must be solved numerically (again using the small-time analysis of Sect. 3 for initial conditions), the ADI scheme used to solve these linear equations is significantly simpler than the full nonlinear computational scheme described in Sect. 5. The agreement between the weakly curved computations and full numerical solutions is demonstrated in Sect. 6.

5 Numerical approach

At finite times we must rely on computational methods to determine the flow. The axial velocity must be evolved using (1*c*), enforcing conditions (2*c*, 11*c*). The axial vorticity must be evolved in accordance with (4*a*), where the boundary and initial conditions for ω are computed via (5), (12) and (4*b*), using ψ from the previous timestep. The stream function for the current timestep is then calculated by inverting (4*b*) whilst satisfying boundary conditions (5). $G(t)$ at the next timestep is determined by enforcing the no-flux condition (6). We discretize our domain into an $N\times N$ uniform grid, approximate spatial derivatives using finite differences and timestep using an ADI scheme. Results were obtained using $N = 100$ and a timestep of $\mathrm{dt} = 10^{-3}$, with numerical convergence verified using $N = 200$ and $\mathrm{dt} = 10^{-3}/2$. Explicit evaluation of the nonlinear terms in the evolution equations, together with the discretized no-flux condition (6), generates a linear system, which we can solve by Gaussian elimination to determine simultaneously, at the next timestep, the axial velocity, axial vorticity, cross-sectional stream function and pressure gradient. The initial condition for the axial pressure gradient is given by the small-time asymptotics developed in Sect. 3, where we chose to timestep from $t = 10^{-3}$ to avoid the singularity at $t = 0$.

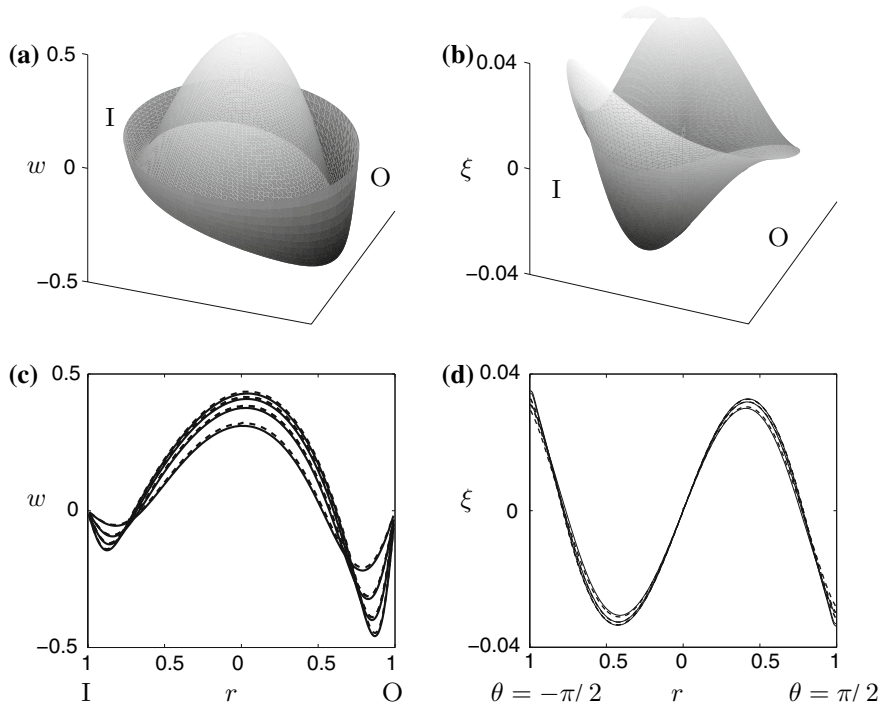

Fig. 2 Suddenly stopped flow in a pipe of curvature $\delta = 0.5$, when the pre-stoppage is driven by an axial pressure gradient of strength $D = -4$. The full profiles for axial flow w and axial vorticity ξ are shown in panels (**a**) and (**b**), respectively, at time $t = 0.004$. Lighter shading indicates positive quantities, while darker shading corresponds to negative quantities. Panels (**c**) and (**d**) plot the numerically computed profile (full line) of w and ξ across the lines $\theta = -\pi, 0$ and $\theta = -\pi/2, \pi/2$, respectively, at times $t = 0.004, 0.006, 0.01, 0.02$ and $0.004, 0.006, 0.01$ (with decreasing magnitude), respectively, alongside the corresponding predictions from the small-time asymptotics (13) (dashed lines). Inner ($\theta = \pi$) and outer pipe ($\theta = 0$) walls are labelled by I and O, respectively

6 Results

We have asserted that understanding the early behaviour of the post-stoppage flow is vital for computing the evolution of the flow at later times; Fig. 2 therefore gauges the effectiveness of the small-time asymptotics derived in Sect. 3. Profiles of the numerically evaluated axial velocity w and axial component of vorticity ξ for flow through a pipe with curvature $\delta = 0.5$ when $D = -4$ (taken along the lines $\theta = (-\pi, 0)$ and $\theta = (-\pi/2, \pi/2)$, respectively), at numerous early times, show the numerical predictions (full lines) to be in good agreement with the asymptotic theory (dashed lines).

For comparison, in Fig. 3 we present the axial velocity profiles for a straight pipe ($\delta = 0$) against one with a high degree of curvature ($\delta = 0.8$). This serves to illustrate the extent to which axi-symmetry in the straight-pipe flow is broken as the pipe becomes curved. We should note, however, that it is by no means clear that the flow will remain fully developed when there is such extreme curvature, so the results relating to such large values of δ should be treated with a degree of caution. Moreover, in the straight-pipe limit (Fig. 3a) we are able to confirm our predictions with those in [16], whilst at large curvature (Fig. 3b) we verify the continued validity of the asymptotic approximations in the small-time limit.

The dramatic influence of curvature at large values of D is revealed in Fig. 4. Flow driven by a high pressure gradient develops thin ($O(\delta^{-1/6}D^{-1/3})$) boundary layers on the pipe wall [6], which collide to form an ejection of fluid from the boundary layer at the circumference on the inner wall soon after the flux is reduced to zero. This jet of reversed flow then proceeds to propogate across the core of the pipe. (Importantly, a similar phenomenon was noted in a physiologically relevant intermittant-flow study [13], where a pulse-like flow rate is followed by a period

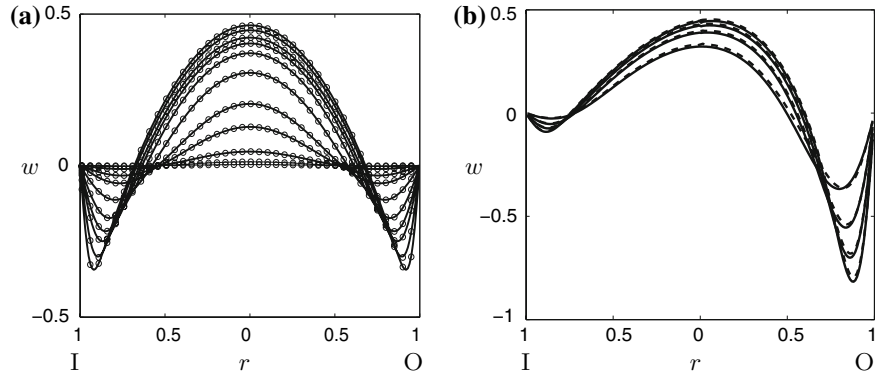

Fig. 3 Profiles of axial flow w taken across the line of horizontal symmetry ($\theta = -\pi, 0$) for (**a**) a straight pipe ($\delta = 0$) and (**b**) a highly curved pipe ($\delta = 0.8$), both with pre-stoppage axial pressure gradient $D = -4$. In (**a**) we compare our numerical predictions (circles) with [16] (full line) at times $t = 0.001, 0.002, 0.004, 0.006, 0.01, 0.02, 0.04, 0.06, 0.1, 0.15$ and 0.2 (top to bottom). For a pipe of finite curvature (b), we compare numerically computed axial flows (full lines) and small-time asymptotics (13) (dashed lines) at time intervals $t = 0.004, 0.006, 0.01, 0.02$ (top to bottom). Inner ($\theta = \pi$) and outer ($\theta = 0$) pipe walls are labelled by I and O, respectively

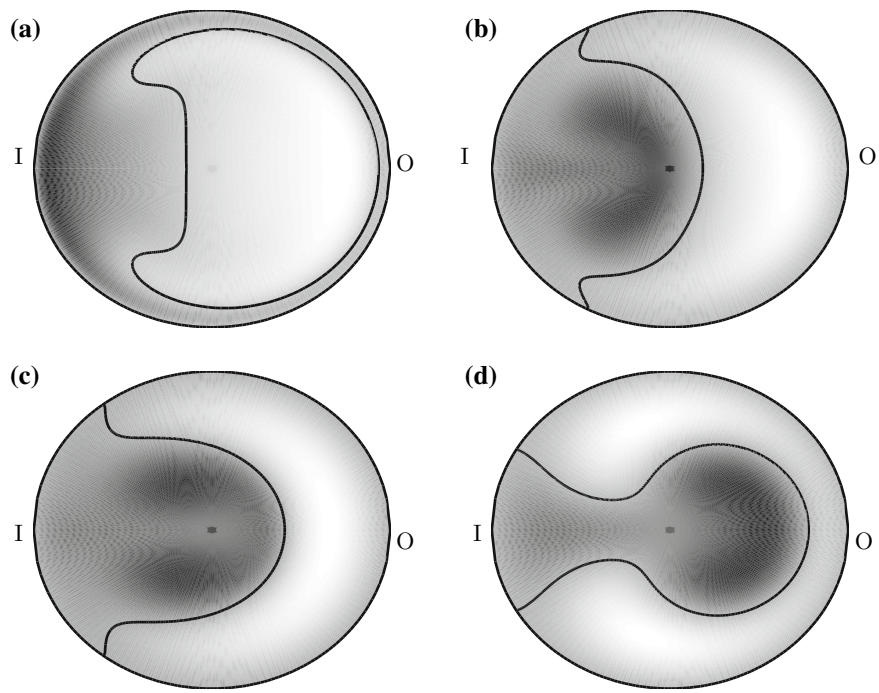

Fig. 4 Axial flow w through the pipe cross-section when $\delta = 0.5$ and $D = -5{,}000$, taken at time (**a**) $t = 10^{-3}$, (**b**) $t = 1.5 \times 10^{-2}$, (**c**) $t = 2.5 \times 10^{-2}$ and (**d**) $t = 5.5 \times 10^{-2}$, showing ejection of fluid into the core of the pipe due to colliding boundary layers. Inner ($\theta = \pi$) and outer ($\theta = 0$) pipe walls are labelled by I and O, respectively. Lighter shading indicates positive axial velocities, while darker shading corresponds to negative quantities. Lines correspond to the $w = 0$ contour

of zero flux.) This large-D effect is compared with the more sedate development of the post-stoppage flow at lower values of D, as shown in Fig. 5.

The consequences of this effect on the life-span of the post-stoppage flow are explored in Fig. 6, where δ is plotted against the time until the maximum axial flow is 1% of its initial, post-stoppage maximum. Decay profiles corresponding to flows with a relatively low value of D are shown in Fig. 6a, to be compared with the large-D case presented in Fig. 6b. In both cases we note the decrease in decay time as the curvature of the pipe is increased,

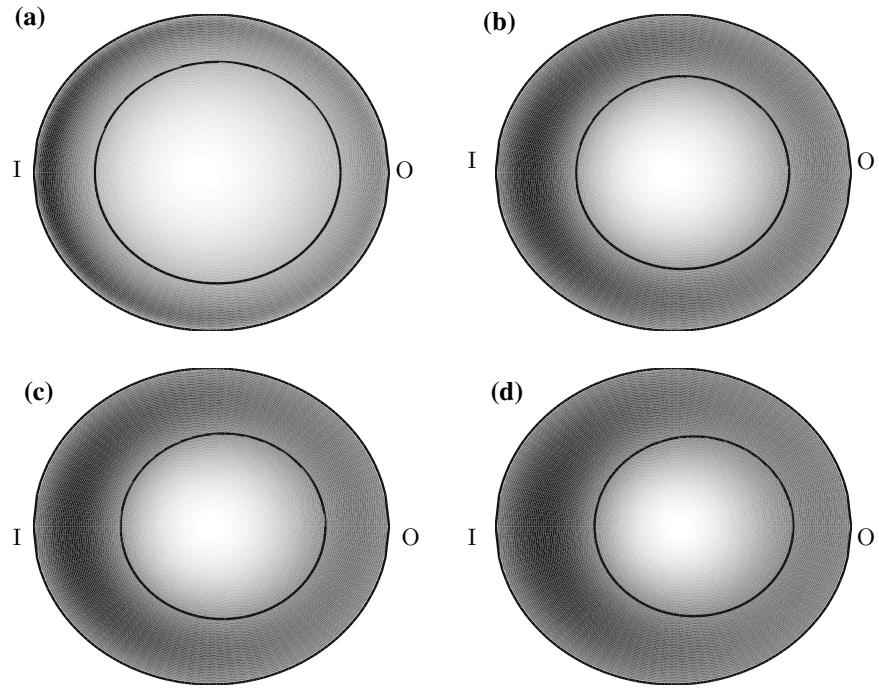

Fig. 5 Axial flow w through the pipe cross-section when $\delta = 0.5$ and $D = -4$, taken at time (**a**) $t = 10^{-3}$, (**b**) $t = 1.5 \times 10^{-2}$, (**c**) $t = 2.5 \times 10^{-2}$ and (**d**) $t = 5.5 \times 10^{-2}$. Inner ($\theta = \pi$) and outer ($\theta = 0$) pipe walls are labelled by I and O, respectively. Lighter shading indicates positive axial velocities, while darker shading corresponds to negative quantities. Lines correspond to the $w = 0$ contour

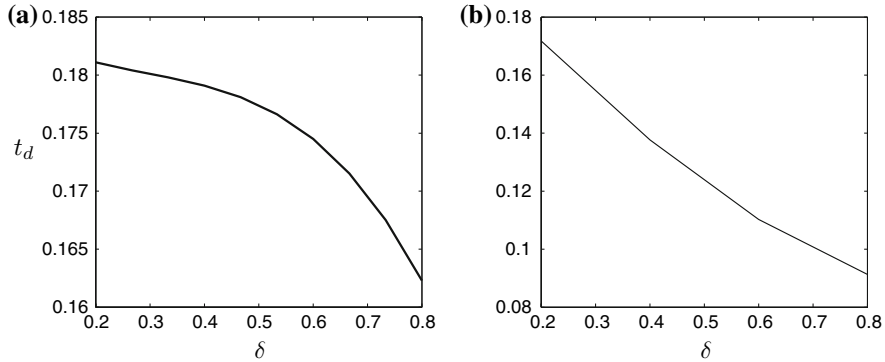

Fig. 6 Plots of δ against the time t_d until the maximum of the post-stoppage axial flow has decayed to 1% of its initial maximum value, for pre-stoppage axial pressure gradients (**a**) $D = -4$ and (**b**) $D = -5{,}000$

which is expected due to the fact that greater curvature results in stronger secondary flows (normalised on their respective axial flows) which, in turn, are more effective at transporting reversed flow from near the walls into the pipe's core. Increases in the relative strength of centrifugally driven flows at large values of D, together with the secondary flows that result from the previously described ejection of fluid from boundary layers that form in the high-D regime, are both likely explanations for the overall reduction in decay times at $D = -5{,}000$ over those observed when $D = -4$.

Finally, as laid out in Sect. 4, in the weak-curvature limit the governing equations can be linearized and Fig. 7 compares the predictions of this weak curvature limit with full numerical computations (when $\delta = 0.1$ and $D = -4$). Here we see the need for inclusion of the leading-order curvature correction w_1 (dashed line) to capture the non-axi-

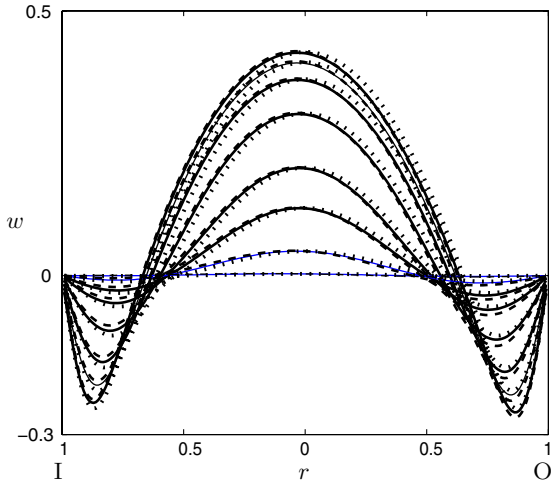

Fig. 7 Profiles of axial flow w taken across the line of horizontal symmetry ($\theta = -\pi, 0$) when $\delta = 0.1$ and $D = -4$ at times $t = 0.004, 0.006, 0.01, 0.02, 0.04, 0.06, 0.1, 0.2$ (top to bottom), together with the straight-pipe axial profile w_0 (dotted line) and the leading-order curvature-corrected flow $w_0 + \delta w_1$ (dashed line) against the full numerical solution (solid line). Inner ($\theta = \pi$) and outer ($\theta = 0$) pipe walls are labelled by I and O, respectively

symmetric character of the decaying axial flow profile, where agreement is observed to be best away from the pipe walls. Furthermore, the overall accuracy of this weak curvature correction appears to be maintained throughout the duration of the flow's post-stoppage decay.

7 Discussion and conclusions

We have examined the decay of initially steady, pressure-driven viscous flow in a finitely curved rigid pipe of uniform cross-section, following the instantaneous imposition of a no-flux condition designed to simulate a sudden blockage of the flow. At sufficiently large distances from the blockage we assume that the flow is fully developed (i.e., does not vary with the axial location). As in the straight-pipe case [12], the axial pressure gradient was an unknown quantity which had to be solved as part of the problem. Initial conditions for the post-stoppage velocity were deduced using the fact that flow vorticity is initially unaffected by the stoppage. Initial conditions for the axial pressure gradient, by contrast, had to be determined through asymptotic analysis of the small-time behaviour of the decaying flow. Equipped with these initial conditions, we solved the flow using an ADI numerical scheme, the results of which were seen to be in good agreement with the asymptotic predictions in the small-time limit. For the case where the pipe was only weakly curved ($\delta \ll 1$), we expanded flow quantities in powers of δ, which lead to a simplified set of linear flow equations and permitted us to use closed-form expressions for the initial flow profile.

The effects of curvature were clearly visible in the non-axisymmetric axial flow profiles, as well as the generation of flows within the pipe's cross-section. Asymptotic analysis showed that the secondary flows decay like $O(t)$ at small times, compared with the more rapid $O(t^{1/2})$ small-time decay of the axial flow.

At high values for the pre-stoppage pressure gradients ($D = -5{,}000$, i.e., representative of blood flow in the human aorta [20]), the influence of pipe curvature was even more pronounced. Once the flow was stopped we observed the propogation of a jet of ejection boundary-layer fluid across the pipe's core (Fig. 4). This effect, also observable in the simulations of aortic blood flow for a less sudden shut-off of the flow rate [13], results from collision of centrifugally driven flows within the boundary layers, which are of thickness $O(\delta^{-1/6}D^{-1/3})$ on the pipe wall, and hence is a product of the pipe's curvature. The finite-time singularity in the unsteady boundary-layer equations which corresponds to this type of boundary-layer collision have recently been characterized mathematically [21], however a mathematical description for the structure of the flow beyond the singularity remains an open problem. (It is also natural to expect that such dramatic jet structures will have important consequences for the stability of the flow beyond the straight-pipe analysis in [14].) The impact of curvature effects upon the rate of decay was clearly illustrated in Fig. 6, with flow through more highly curved pipes decaying more rapidly, presumably due to the associated enhancement of secondary flows and accompanying improvement of the flow's transport properties.

This trend was seen to be more pronounced as D was increased, where centrifugally driven secondary flows are augmented by the aforementioned ejection of fluid from the colliding boundary layers.

Acknowledgements This work was supported by Australian Research Council grant DP0556360. We are grateful to Jonathan Mestel for his comments on the original manuscript.

Appendix A: Small-time flow structure

We here give details of the flows in the core of the pipe and within diffusive boundary layers on the pipe wall, which match together to form the uniformly valid expansion given by (13) in Sect. 3.

A.1 Core flow

From (1), the $O(1)$ core velocity $\hat{\boldsymbol{u}}^{(0)}$ satisfies

$$\partial_T \hat{u}^{(0)} = \partial_T \hat{v}^{(0)} = 0, \quad \partial_T \hat{w}^{(0)} = \frac{G^{(0)}(T)}{h}.$$

Noting that the $O(1)$ flux is proportional to the integral of $G^{(0)}$ over time, $Q(T) \propto \int_0^T G^{(0)}(T')\mathrm{d}T' + O(\epsilon^{1/2})$, the zero-flux condition therefore requires

$$G^{(0)}(T) = 0. \tag{19a}$$

The initial conditions (11) now give

$$\begin{aligned} &\hat{u}^{(0)}(r,\theta,T) = u_D(r,\theta), \quad \hat{v}^{(0)}(r,\theta,T) = v_D(r,\theta), \\ &\hat{w}^{(0)}(r,\theta,T) = w_D(r,\theta) - \alpha h^{-1}. \end{aligned} \tag{19b}$$

However, these solutions generate an axial slip velocity $\hat{w}^{(0)} = -\alpha h_1^{-1}$ at the wall ($r = 1$), where $h_1 = 1 + \delta\cos\theta$. This is reconciled with the no-slip condition via a boundary-layer flow $\tilde{\boldsymbol{u}}^{(0)}$, considered in Sect. A.2, which forms on the pipe wall immediately after the flow's stoppage. The boundary-layer flow $\tilde{\boldsymbol{u}}^{(0)}$ generates an $O(\epsilon^{1/2})$ flux, denoted $Q^{(00)}$ (see (14)), however, which drives an $O(\epsilon^{1/2})$ core flow $\hat{\boldsymbol{u}}^{(1)}$.

We therefore seek a first-order correction to the core flow with the form

$$\hat{\boldsymbol{u}}^{(1)}(r,\theta,T) = T^{1/2}\hat{\boldsymbol{U}}^{(1)}(r,\theta)$$

which, as we shall see in Sect. A.2, exhibits the required time dependence to cancel the flux due to $\tilde{\boldsymbol{u}}^{(0)}$. From (1$c$), the $O(\epsilon^{1/2})$ flow is driven by an $O(\epsilon^{-1/2})$ axial pressure gradient with the form

$$G^{(1)}(T) = T^{-1/2}\bar{G}^{(1)}.$$

This leads to

$$\partial_T \hat{U}^{(1)} = \partial_T \hat{V}^{(1)} = 0, \quad \partial_T\left(T^{1/2}\hat{W}^{(1)}\right) = h^{-1}T^{-1/2}\bar{G}^{(1)}, \tag{20}$$

hence

$$\hat{U}^{(1)} = \hat{V}^{(1)} = 0, \quad \hat{W}^{(1)} = 2h^{-1}\bar{G}^{(1)}. \tag{21}$$

The exact form of $\bar{G}^{(1)}$ must be computed such that no-flux is enforced at $O(\epsilon^{1/2})$ (see Sect. 3). The axial flow $\hat{W}^{(1)}$ generates a slip velocity $2T^{1/2}h_1^{-1}\bar{G}^{(1)}$ at the wall, which is adjusted to zero by the $O(\epsilon^{1/2})$ correction $\tilde{\boldsymbol{u}}^{(1)}$ to the boundary-layer flow. This boundary-layer flow $\tilde{\boldsymbol{u}}^{(1)}$, in turn, generates an $O(\epsilon)$ flux which must be corrected by an $O(\epsilon)$ core flow.

Prescribing the time dependence

$$\hat{\boldsymbol{u}}^{(2)}(r,\theta,T) = T\hat{\boldsymbol{U}}^{(2)}(r,\theta) \tag{22}$$

(which also implies that $G^{(2)}$ is time-independent), we obtain

$$\hat{U}^{(2)} = -u_D\partial_r u_D - \frac{v_D\partial_\theta u_D}{r} + \frac{v_D^2}{r} + \frac{\delta\cos\theta\left(\hat{w}^{(0)}\right)^2}{h} - \partial_r\hat{p}^{(2)}$$
$$-\frac{1}{rh}\partial_\theta\left[h\left(\partial_r v_D + \frac{v_D}{r} - \frac{\partial_\theta u_D}{r}\right)\right] = -\partial_r\hat{P}^{(2)} - \frac{\delta\cos\theta}{h^2}\left(2\alpha w_D - \frac{\alpha^2}{h}\right), \tag{23a}$$

$$\hat{V}^{(2)} = -u_D\partial_r v_D - \frac{v_D\partial_\theta v_D}{r} - \frac{u_D v_D}{r} - \frac{\delta\sin\theta\left(\hat{w}^{(0)}\right)^2}{h} - \frac{\partial_\theta\hat{p}^{(2)}}{r}$$
$$+\frac{1}{h}\partial_r\left[h\left(\partial_r v_D + \frac{v_D}{r} - \frac{\partial_\theta u_D}{r}\right)\right] = -\frac{\partial_\theta\hat{P}^{(2)}}{r} + \frac{\delta\sin\theta}{h^2}\left(2\alpha w_D - \frac{\alpha^2}{h}\right), \tag{23b}$$

using the governing equations for the pre-stoppage flow with

$$\hat{p}^{(2)} = p_D + \hat{P}^{(2)},$$

where p_D is the cross-sectional pressure for the pre-stoppage flow and $\hat{P}^{(2)}$ is chosen to enforce conservation of mass

$$\nabla^2\hat{P}^{(2)} \equiv \frac{1}{rh}\left(\partial_r\left(rh\partial_r\hat{P}^{(2)}\right) + \partial_\theta\left(\frac{h}{r}\partial_\theta\hat{P}^{(2)}\right)\right) = \frac{\delta^2}{h^3}H(r,\theta) + \frac{\delta}{h^2}\left(\frac{\sin\theta}{r}\partial_\theta H(r,\theta) - \cos\theta\partial_r H(r,\theta)\right), \tag{23c}$$

where

$$H(r,\theta) = \left(2\alpha w_D - \frac{\alpha^2}{h}\right),$$

subject to

$$\partial_r\hat{P}^{(2))}(1,\theta) = -\frac{\delta\cos\theta}{h_1^2}\left(2\alpha w_D(1,\theta) - \frac{\alpha^2}{h_1}\right) = \frac{\alpha^2\delta\cos\theta}{h_1^3} \tag{23d}$$

(from the no-penetration condition $\hat{U}^{(2)}(1,\theta) = 0$). This, in turn, implies that the $O(\epsilon)$ axial component of flow vorticity in the core of the pipe takes the form

$$\hat{\xi}^{(2)} = \frac{2\alpha\delta T}{h^2}\left(\sin\theta\partial_r w_D + \frac{\cos\theta}{r}\partial_\theta w_D\right).$$

In terms of the axial flow,

$$\hat{W}^{(2)} = -u_D\partial_r\hat{w}^{(0)} - \frac{v_D\partial_\theta\hat{w}^{(0)}}{r}$$
$$-\frac{\delta\cos\theta u_D\hat{w}^{(0)}}{h} + \frac{\delta\sin\theta v_D\hat{w}^{(0)}}{h} + \frac{G^{(2)}}{h} + \mathcal{L}^2\hat{w}^{(0)} = \frac{G^{(2)}}{h} - \frac{D}{h}, \tag{23e}$$

(since $\mathcal{L}^2(\alpha/h) = 0$ and so $\mathcal{L}^2\hat{w}^{(0)} = \mathcal{L}^2 w_D$) where $G^{(2)}$ is computed such that no-flux is ensured at $O(\epsilon)$ (see Sect. 3).

So from (19), (21) and (23) we obtain the outer flow (correct up to $O(\epsilon^{3/2})$)

$$\hat{u} = u_D + t\left[-\partial_r\hat{P}^{(2)} - \frac{2\alpha\delta\cos\theta w_D}{h^2} + \frac{\alpha^2\delta\cos\theta}{h^3}\right], \tag{24a}$$

$$\hat{v} = v_D + t\left[-\frac{1}{r}\partial_\theta\hat{P}^{(2)} + \frac{2\alpha\delta\sin\theta w_D}{h^2} - \frac{\alpha^2\delta\sin\theta}{h^3}\right], \tag{24b}$$

$$\hat{w} = \left(w_D - \frac{\alpha}{h}\right) + t^{1/2}\frac{2\bar{G}^{(1)}}{h} + t\left[\frac{G^{(2)}}{h} - \frac{D}{h}\right], \tag{24c}$$

$$\hat{\xi} = \xi_D + t\left[\frac{2\alpha\delta}{h^2}\left(\sin\theta\partial_r w_D + \frac{\cos\theta}{r}\partial_\theta w_D\right)\right], \tag{24d}$$

($\xi_D = -\mathcal{L}^2\psi_D$ where $\Psi_D = h\psi_D$). In terms of the boundary-layer variable

$$\eta = \frac{1}{2}t^{-1/2}(1-r),$$

the inner limit of the flow, correct up to $O(\epsilon^{3/2})$, is therefore

$$\hat{u} \to -2\eta t^{1/2}\partial_r u_D(1,\theta) + 2\eta^2 t\partial^2_{rr}u_D(1,\theta) = 2\eta^2 t\partial^2_{rr}u_D(1,\theta), \tag{25a}$$

$$\hat{v} \to -2\eta t^{1/2}\partial_r v_D(1,\theta) + t\left[-\partial_\theta \hat{P}^{(2)} + 2\eta^2\partial^2_{rr}v_D(1,\theta) - \frac{\alpha^2\delta\sin\theta}{h_1^3}\right], \tag{25b}$$

$$\begin{aligned}\hat{w} \to\ & -\frac{\alpha}{h_1} + t^{1/2}\left[\frac{2\bar{G}^{(1)}}{h_1} - 2\eta\partial_r w_D(1,\theta) - \frac{2\alpha\eta\delta\cos\theta}{h_1^2}\right] \\ & + t\left[\frac{G^{(2)}}{h_1} - \frac{4\alpha\eta^2\delta^2\cos^2\theta}{h_1^3} + 2\eta^2\partial^2_{rr}w_D(1,\theta) - \frac{D}{h_1} + \frac{4\delta\bar{G}^{(1)}\eta\cos\theta}{h_1^2}\right],\end{aligned} \tag{25c}$$

where we have used the fact that $\partial_r u_D(1,\theta) = 0$ from the continuity equation, and the inner limit of the pressure (up to $O(\epsilon)$ corrections) is

$$\hat{p}^{(2)} \to \left(p_D(1,\theta) + \hat{P}^{(2)}(1,\theta)\right) - 2\eta t^{1/2}\left(\partial_r p_D(1,\theta) + \partial_r\hat{P}(1,\theta)\right). \tag{25d}$$

We next discuss the boundary-layer flow that matches onto this core flow.

A.2 Boundary-layer flow

From (1), the leading-order boundary-layer flow $\tilde{\boldsymbol{u}}^{(0)}$ satisfies

$$\begin{aligned}&\partial_T\tilde{u}^{(0)} - \frac{1}{2}T^{-1}\eta\partial_\eta\tilde{u}^{(0)} = 0, \quad \partial_T\tilde{v}^{(0)} - \frac{1}{2}T^{-1}\eta\partial_\eta\tilde{v}^{(0)} - \frac{1}{4}T^{-1}\partial^2_{\eta\eta}\tilde{v}^{(0)} = 0,\\ &\partial_T\tilde{w}^{(0)} - \frac{1}{2}T^{-1}\eta\,\partial_\eta\tilde{w}^{(0)} = \frac{1}{4}T^{-1}\partial^2_{\eta\eta}\tilde{w}^{(0)},\end{aligned} \tag{26a}$$

subject to the matching condition (25)

$$\tilde{\boldsymbol{u}}^{(0)}(0,\theta,t) = \boldsymbol{0}, \quad \tilde{u}^{(0)}(\eta,\theta,t), \tilde{v}^{(0)}(\eta,\theta,t) \to 0, \tag{26b}$$

$$\tilde{w}^{(0)}(\eta,\theta,t) \to -\alpha h_1^{-1} \quad \text{as } \eta\to\infty. \tag{26c}$$

Hence (26) is solved by

$$\tilde{u}^{(0)} = \tilde{v}^{(0)} = 0, \quad \tilde{w}^{(0)} = -\alpha h_1^{-1}\mathrm{erf}(\eta), \tag{27}$$

where $\mathrm{erf}(\eta)$ is the Error Function. The boundary-layer flow $\tilde{\boldsymbol{u}}^{(1)}$ at $O(\epsilon^{1/2})$ satisfies

$$\partial_T\tilde{u}^{(1)} - \frac{1}{2}T^{-1}\eta\partial_\eta\tilde{u}^{(1)} = \frac{1}{2}T^{-1/2}\partial_\eta\tilde{p}^{(2)}, \tag{28a}$$

$$\partial_T\tilde{v}^{(1)} - \frac{1}{2}T^{-1}\eta\partial_\eta\tilde{v}^{(1)} = \frac{1}{4}T^{-1}\partial^2_{\eta\eta}\tilde{v}^{(1)}, \tag{28b}$$

$$\begin{aligned}&\partial_T\tilde{w}^{(1)} - \frac{1}{2}T^{-1}\eta\partial_\eta\tilde{w}^{(1)} - \frac{1}{2}T^{-1/2}\tilde{u}^{(0)}\partial_\eta\tilde{w}^{(0)} \\ &\quad = \frac{T^{-1/2}\bar{G}^{(1)}}{h_1} + \frac{1}{4}T^{-1}\partial^2_{\eta\eta}\tilde{w}^{(1)} - \frac{1}{2}T^{-1/2}\left(\frac{1+2\delta\cos\theta}{h_1}\right)\partial_\eta\tilde{w}^{(0)}.\end{aligned} \tag{28c}$$

Prescribing an explicit time-dependence which is consistent with the core flow,

$$\tilde{\boldsymbol{u}}^{(1)}(\eta,\theta,T) = T^{1/2}\tilde{\boldsymbol{U}}^{(1)}(\eta,\theta)$$

and using the fact that $\tilde{u}^{(0)}(\eta,\theta,T)=0$, we obtain

$$\partial^2_{\eta\eta}\tilde{W}^{(1)}+2\eta\partial_\eta\tilde{W}^{(1)}-2\tilde{W}^{(1)}=-\frac{4\bar{G}^{(1)}}{h_1}+2\left(\frac{1+2\delta\cos\theta}{h_1}\right)\partial_\eta\tilde{w}^{(0)}$$
$$=-\frac{4\bar{G}^{(1)}}{h_1}-\frac{4\alpha(1+2\delta\cos\theta)e^{-\eta^2}}{\sqrt{\pi}h_1^2}. \tag{29}$$

We can solve (28a,b) and (29), subject to $\tilde{W}^{(1)}(0,\theta)=0$ and the matching condition (25), to yield

$$\tilde{U}^{(1)}(\eta,\theta)=0,\quad \tilde{V}^{(1)}(\eta,\theta)=-2\eta\partial_r v_D(1,\theta), \tag{30a}$$

$$\tilde{W}^{(1)}(\eta,\theta)=\frac{2\bar{G}^{(1)}}{h_1}\left(1-e^{-\eta^2}+\sqrt{\pi}\eta\,\mathrm{erfc}\eta\right)+\frac{\alpha(1+2\delta\cos\theta)}{h_1^2}\eta\,\mathrm{erfc}\eta$$
$$-2\eta\left(\partial_r w_D(1,\theta)+\frac{\alpha\delta\cos\theta}{h_1^2}\right), \tag{30b}$$

$$\partial_\eta\tilde{p}^{(2)}=0 \text{ implying that } \tilde{p}^{(2)}=p_D(1,\theta)+\tilde{P}^{(2)}(1,\theta), \tag{30c}$$

where $\mathrm{erfc}(\eta)=1-\mathrm{erf}(\eta)$ is the Complementary Error Function.

The $O(\epsilon)$ boundary-layer flow $\tilde{\boldsymbol{u}}^{(2)}$, which is prescribed the time dependence

$$\tilde{\boldsymbol{u}}^{(2)}(r,\theta,T)=T\tilde{\boldsymbol{U}}^{(2)}(r,\theta),$$

satisfies

$$\tilde{U}^{(2)}-\frac{1}{2}\eta\partial_\eta\tilde{U}^{(2)}=\frac{1}{2}\partial_\eta\tilde{p}^{(3)}+\frac{1}{2t^{1/2}}\partial_\theta\partial_\eta\tilde{v}^{(1)}-\frac{\delta\sin\theta}{2h_1t^{1/2}}\partial_\eta v^{(1)}+\frac{\delta\cos\theta\left(w^{(0)}\right)^2}{h_1}$$
$$=\frac{1}{2}\partial_\eta\tilde{p}^{(3)}+\partial^2_{rr}u_D(1,\theta)+\frac{\delta\cos\theta\left(w^{(0)}\right)^2}{h_1}\text{ from the continuity equation}$$
$$=\frac{1}{2}\partial_\eta\tilde{P}^{(3)}-\partial_r\hat{P}^{(2)}(1,\theta)+\frac{\delta\cos\theta\left(w^{(0)}\right)^2}{h_1}=\frac{1}{2}\partial_\eta\tilde{P}^{(3)}+\frac{\alpha^2\delta\cos\theta\left((\mathrm{erf}\eta)^2-1\right)}{h_1^3}$$

where

$$\tilde{p}^{(3)}=-2\eta\left(\partial_r p_D(1,\theta)+\partial_r\hat{P}^{(2)}(1,\theta)\right)+\tilde{P}^{(3)}.$$

However, conservation of mass demands that

$$\partial_\eta\tilde{U}^{(2)}=2\left(\partial_\theta\tilde{V}^{(1)}-\frac{\delta\sin\theta\tilde{V}^{(1)}}{h_1}\right)=-4\eta\left(\partial_\theta\partial_r v_D(1,\theta)-\frac{\delta\sin\theta\partial_r v_D(1,\theta)}{h_1}\right)=-4\eta\partial^2_{rr}u_D(1,\theta),$$

implying that

$$\tilde{U}^{(2)}=-2\eta^2\partial_{rr}u_D(1,\theta) \tag{31a}$$

(taking into consideration the no-penetration condition). Hence

$$\tilde{U}^{(2)}-\frac{1}{2}\eta\partial_\eta\tilde{U}^{(2)}=0$$

and

$$\partial_\eta\tilde{P}^{(3)}=-\frac{2\alpha^2\delta\cos\theta\left((\mathrm{erf}\eta)^2-1\right)}{h_1^3}.$$

The two other flow velocity components satisfy

$$\begin{aligned}\tilde{V}^{(2)}-\frac{1}{2}\eta\partial_\eta\tilde{V}^{(2)}-\frac{1}{4}\partial^2_{\eta\eta}\tilde{V}^{(2)} &= -\partial_\theta\tilde{p}^{(2)}-\frac{1}{2t^{1/2}}\left(1+\frac{\delta\cos\theta}{h_1}\right)\partial_\eta\tilde{V}^{(1)}-\frac{\delta\sin\theta\left(\tilde{w}^{(0)}\right)^2}{h_1}\\ &= -\partial_\theta\tilde{p}^{(2)}+\left(1+\frac{\delta\cos\theta}{h_1}\right)\partial_r v_D(1,\theta)-\frac{\alpha^2\delta\sin\theta\,(\mathrm{erf}\eta)^2}{h_1^3}\\ &= -\partial_\theta\hat{P}^{(2)}(1,\theta)-\partial_\theta p_D(1,\theta)+\left(1+\frac{\delta\cos\theta}{h_1}\right)\partial_r v_D(1,\theta)-\frac{\alpha^2\delta\sin\theta\,(\mathrm{erf}\eta)^2}{h_1^3}\\ &= -\partial_\theta\hat{P}^{(2)}(1,\theta)-\partial^2_{rr}v_D(1,\theta)-\frac{\alpha^2\delta\sin\theta\,(\mathrm{erf}\eta)^2}{h_1^3} \qquad (31b)\end{aligned}$$

and

$$\begin{aligned}\tilde{W}^{(2)}-\frac{1}{2}\eta\partial_\eta\tilde{W}^{(2)}-\frac{1}{4}\partial_{\eta\eta}\tilde{W}^{(2)} &= \frac{2\bar{G}^{(1)}\eta\delta\cos\theta}{h_1^2}-\left(\frac{1+2\delta\cos\theta}{2h_1}\right)\partial_\eta\tilde{W}^{(1)}-\left(1+\frac{\delta^2\cos^2\theta}{h_1^2}\right)\eta\partial_\eta\tilde{w}^{(0)}\\ &\quad+\partial_{\theta\theta}\tilde{w}^{(0)}-\frac{\delta\sin\theta}{h_1}\partial_\theta\tilde{w}^{(0)}-\frac{\delta^2}{h_1^2}\tilde{w}^{(0)}+\frac{G^{(2)}}{h_1}\\ &= \frac{2\bar{G}^{(1)}\eta\delta\cos\theta}{h_1^2}+\frac{G^{(2)}}{h_1}+2f_2(\theta)\eta e^{-\eta^2}\\ &\quad-\left(\frac{\alpha}{2h_1^3}(1+2\delta\cos\theta)+\frac{\bar{G}^{(1)}\sqrt{\pi}(1+2\delta\cos\theta)}{h_1^2}\right)\mathrm{erfc}\eta\\ &\quad+\left(\frac{1+2\delta\cos\theta}{h_1}\right)\partial_r w_D(1,\theta)+\frac{2\alpha\delta^2\cos^2\theta\,\mathrm{erf}\eta}{h_1^3}, \qquad (31c)\end{aligned}$$

where

$$f_2(\theta)=\alpha\pi^{-1/2}h_1^{-3}\left(\frac{3}{2}+4\delta\cos\theta+4\delta^2\cos^2\theta\right). \qquad (32)$$

The required axial flow which satisfies $\tilde{W}^{(2)}(0)=0$ and (25) is given by

$$\tilde{U}^{(2)} = 2\eta^2\partial^2_{rr}u_D(1,\theta), \qquad (33a)$$

$$\tilde{V}^{(2)} = 2\eta^2\partial^2_{rr}v_D(1,\theta)-\partial_\theta\hat{P}^{(2)}(1,\theta)+K(\eta,\theta), \qquad (33b)$$

$$\begin{aligned}\tilde{W}^{(2)} &= \frac{4\delta\bar{G}^{(1)}\eta\cos\theta}{h_1^2}+f_2(\theta)\eta e^{-\eta^2}-\frac{2\alpha\delta^2\cos^2\theta}{h_1^3}\left(2\eta^2\mathrm{erf}\eta+\frac{2\eta e^{-\eta^2}}{\sqrt{\pi}}\right)\\ &\quad+A_1(r,\theta)\left(\frac{2\eta e^{-\eta^2}}{\sqrt{\pi}}-2\eta^2\mathrm{erfc}\eta\right)+A_2(r,\theta)\left(1-(1+2\eta^2)\mathrm{erfc}\eta+\frac{2\eta e^{-\eta^2}}{\sqrt{\pi}}\right)\\ &\quad+\partial^2_{rr}w_D(1,\theta)\left((1+2\eta^2)\mathrm{erf}\eta+\frac{2\eta e^{-\eta^2}}{\sqrt{\pi}}\right) \qquad (33c)\end{aligned}$$

where

$$A_1(r,\theta)=-\left(\frac{\alpha}{2h_1^3}(1+2\delta\cos\theta)+\frac{\bar{G}^{(1)}\sqrt{\pi}(1+2\delta\cos\theta)}{h_1^2}\right), \qquad (34a)$$

$$A_2(r,\theta)=+\left(\frac{G^{(2)}}{h_1}+\left(\frac{1+2\delta\cos\theta}{h_1}\right)\partial_r w_D(1,\theta)\right). \qquad (34b)$$

$K(\eta, \theta)$ is a function, which must be found numerically, satisfying

$$K - \frac{1}{2}\eta\partial_\eta K - \frac{1}{4}\partial^2_{\eta\eta} K = -\frac{\alpha^2\delta \sin\theta (\mathrm{erf}\eta)^2}{h_1^3}, \tag{35}$$

subject to

$$K(0, \theta) = \partial_\theta \hat{P}^{(2)}(1, \theta), \quad K(\eta, \theta) \to -\frac{\alpha^2\delta \sin\theta}{h_1^3} \quad \text{as } \eta \to \infty.$$

References

1. Pedley TJ (2003) Mathematical modelling of arterial fluid dynamics. J Eng Math 47:419–444
2. Caro CG, FitzGerald JM, Schroter RC (1971) Atheroma and arterial wall shear—observation, correlation and proposal of a shear dependent mass transfer mechanism for atherogenesis. Proc R Soc London Ser B 177:109
3. Dean WR (1928) The stream-line motion of fluid in a curved pipe. Philos Mag 5:673–695
4. Pedley TJ, Kamm RD (1988) The effect of secondary motion of axial transport in oscillatory tube flow. J Fluid Mech 193:347–367
5. Dennis SCR, Ng M (1982) Dual solutions for steady laminar-flow through a curved tube. Q J Mech Appl Math 35:305–324
6. Siggers JH, Waters SL (2005) Steady flows in pipes with finite curvature. Phys Fluid 17:077102
7. Zabielski L, Mestel AJ (1998) Unsteady blood flow in a helically symmetric pipe. J Fluid Mech 10:321–345
8. Waters SL, Pedley TJ (1999) Oscillatory flow in a tube of time-dependent curvature. Part 1. Perturbation to flow in a stationary curved tube. J Fluid Mech 383:327–352
9. Lyne WH (1971) Unsteady viscous flow in a curved pipe. J Fluid Mech 45:13–31
10. Smith FT (1975) Pulsatile flow in curved pipes. J Fluid Mech 71:15–42
11. Chang LJ, Tarbell JM (1985) Numerical-simulations of fully-developed sinusoidal and pulsatile (physiological) flow in curved tubes. J Biomech 12:793–805
12. Weinbaum S, Parker KH (1975) The laminar decay of suddenly blocked channel and pipe flows. J Fluid Mech 69:729–752
13. Komai Y, Tanishita K (1997) Fully developed intermittent flow in a curved tube. J Fluid Mech 347:263–287
14. Hall P, Parker KH (1976) The stability of the decaying flow in a suddenly blocked channel. J Fluid Mech 75:305–314
15. Trefethen LN, Trefethen AE, Reddy SC, Driscoll TA (1993) Hydrodynamic stability without eigenvalues. Science 261:578–584
16. Jewell N, Denier JP (2006) The instability of the flow in a suddenly blocked pipe. QJMAM 59:651–673
17. Liggett JA, Chen LC (1994) Inverse transient analysis in pipe networks. J Hydraul Eng 120:934–955
18. Ghidaoui MS, Mansour S (2002) Efficient treatment of the Vardy-Brown unsteady shear in pipe transients. J Hydraul Eng 128:102–112
19. Pedley TJ (1980) The fluid mechanics of large blood vessels. Cambridge University Press
20. Yearwood TL, Chandran KB (1982) Physiological pulsatile flow experiments in a model of the human aortic arch. J Biomech 15:683
21. Riley N (1998) Unsteady fully developed flow in a curved pipe. J Eng Math 34:131–141